Journal of Structural Biology: X 9 (2024) 100098

Contents lists available at ScienceDirect

Journal of Structural Biology: X

journal homepage: www.sciencedirect.com/journal/journal-of-structural-biology-x

Magic-angle spinning NMR structure of Opa60 in lipid bilayers

Marcel C. Forster, Kumar Tekwani Movellan, Eszter E. Najbauer, Stefan Becker, Loren B. Andreas *

Department of NMR-based Structural Biology, Max-Planck-Institute for Multidisciplinary Sciences, Am Faßberg 11, 37077 Göttingen, Germany

ARTICLE INFO

Keywords:
Solid-state NMR
Membrane protein
Magic-angle spinning
Opacity associated protein
Atomic resolution structure

ABSTRACT

Here we report the structure of Opa60 in lipid bilayers using proton-detected magic-angle spinning nuclear magnetic resonance (MAS NMR). Preparations including near-native oligosaccharide lipids reveal a consistent picture of a stable transmembrane beta barrel with a minor increase in the structured region as compared with the previously reported detergent structure. The large variable loops known to interact with host proteins could not be detected, confirming their dynamic nature even in a lipid bilayer environment. The structure provides a starting point for investigation of the functional role of Opa60 in gonococcal infection, which is understood to involve interaction with host proteins. At the same time, it demonstrates the recent advances in proton-detected methodology for membrane protein structure determination at atomic resolution by MAS NMR.

Introduction

Structural characterization of membrane proteins is of high interest due to their importance in living organisms. Membrane proteins account for about 60% of drug targets (Overington et al., 2006), as their functions range from signal transduction, through transportation of metabolites and ions, to enzymatic activity (Cournia et al., 2015; Wimley, 2003; Galdiero et al., 2007). Conventional approaches to determine membrane protein structure, such as crystallization(Kwan et al., 2020) or solution nuclear magnetic resonance (NMR) spectroscopy (Tamm and Liang, 2006) typically take place in the presence of detergents, which may alter the protein's native structure (Chipot et al., 2018; Schubeis et al., 2020; Zhou and Cross, 2013), while cryo electron microscopy is not suited for the study of small proteins (Cheng, 2018). In contrast, magic angle spinning (MAS) NMR spectroscopy offers a unique opportunity to study small membrane proteins at atomic detail in a native-like lipid bilayer environment (Schubeis et al., 2018; Xue et al., 2021; Mandala et al., 2018). The lipid composition of native bacterial membranes is highly diverse (Sohlenkamp and Geiger, 2016), and lipid composition is known to impact membrane protein structure and function (Thakur et al., 2023). Moreover, bacterial outer membranes feature a high amount of structurally and functionally important lipopolysaccharides (LPS) or lipooligosaccharides (LOS) (Raetz and Whitfield, 2002; Wilkinson, 1996), which can be incorporated into lipid preparations for MAS NMR. In addition to structural characterization, NMR spectroscopy can also offer atomic resolution insight into the dynamic behavior of proteins on different physiologically relevant timescales (Schanda and Ernst, 2016). As particularly dynamic regions of the protein are not detected in cross-polarization based NMR spectra, undetected regions of the protein can be easily identified as mobile (Matlahov and van der Wel, 2018).

Opacity associated (Opa) proteins form a large group of beta barrel outer membrane proteins found in bacterial pathogens of the *Neisseria* genus (Hobbs et al., 1994; Malorny et al., 1998). They bind to human epithelial host tissues via interaction with the carcinoembryonic antigen-related cell adhesion molecule (CEACAM) or the heparan sulfate proteoglycan (HSPG) family of proteins and mediate infection of human hosts (Hauck and Meyer, 2003; Gray-Owen, 2003; Criss and Seifert, 2012). Structural elucidation of these interactions will likely be key to understanding pathogenicity.

Structurally, all Opa proteins are eight stranded beta barrels with four extracellular loops. The structure of Opa60 (~28 kDa) from *N. gonorrhoeae* has been determined previously in dodecylphosphocholine (DPC) detergent micelles using solution NMR (Fox et al., 2014; Fox and Columbus, 2013). The structure of the transmembrane beta barrel was reported, and about 95% of the transmembrane region and 27% of the loops were assigned. The extracellular loops feature three variable regions, termed semivariable (SV) and hypervariable (HV) 1 and 2 regions. Of these, both large HV regions confer receptor binding and specificity, and it has been shown that only the precise combinations of

* Corresponding author.
E-mail address: land@mpinat.mpg.de (L.B. Andreas).

https://doi.org/10.1016/j.yjsbx.2024.100098
Received 7 November 2023; Received in revised form 30 January 2024; Accepted 19 February 2024
Available online 21 February 2024

HV1 and HV2 loops are able to mediate the specific binding to host receptor proteins (de Jonge et al., 2003). The HV1 and HV2 loops exhibited dynamics on the nanosecond timescale, and showed short-lived interactions with each other and the adoption of helical secondary structures in a minority of MD simulation snapshots (Fox et al., 2014).

Opa proteins differ mostly in their HV regions (Malorny et al., 1998). For meningococcal Opa variants, a conserved sequence on HV2 has been found. It has also been shown that the binding depends on the combination of HV1 and HV2 sequences, such that chimeric sequences do not necessarily bind (de Jonge et al., 2003; Bos et al., 2002). The binding of Opa proteins to CEACAMs and HSPGs has been studied extensively by a chimeric protein approach (Bos et al., 2002) and recently also by fluorescence activated cell sorting (FACS) (Werner et al., 2020). The affinity of Opa proteins to CEACAM receptors has been reported to be in the low nanomolar range (Martin et al., 2016).

Here we report the structure of Opa60 in 1,2-dimyristoyl-*sn*-glycero-3-phosphocholine (DMPC) lipid bilayers using proton-detected MAS NMR. Using a semi-automated assignment strategy, we obtained comprehensive assignments for the beta barrel of the protein and determined that while the structured region of the beta barrel is somewhat larger in comparison to the detergent structure, the loops retain their mobility in a lipid membrane environment.

Materials and methods

Opa60 sample preparation

The procedure for production, purification, and lipid reconstitution of Opa60 was published before (Zhang et al., 2021) and is based on an earlier report (Fox et al., 2014). A pET-28b(+) plasmid containing the Opa60 sequence was transformed into *Escherichia coli* BL21 (DE3) cells. Fully ^{2}H, ^{13}C, ^{15}N-labelled Opa60 was expressed in M9 medium containing 100% D_2O, 4 g/l $^{13}C_6$-d$_7$-D-glucose and 1 g/l ^{15}N-NH_4Cl. Cells were grown to an OD_{600} of ~ 0.8 at 37 °C. Before induction, the temperature was decreased to 25 °C. Expression was induced with 1 mM isopropyl-β-D-1-thiogalactopyranoside (IPTG). After overnight expression, cells were harvested by centrifugation for 20 min at 5,000 g and 4 °C. The pellet was resuspended in ~ 35 ml lysis buffer (50 mM Tris, 150 mM NaCl, 1 mM $MgCl_2$, pH 8.0, cOmplete™ EDTA-free protease inhibitor cocktail (Roche)). Bacteria were lysed by digestion with 25 μg DNase/Lysozyme each for 30 min at room temperature, followed by sonication (Sonopuls HD 2200 (Bandelin), 6x60% of maximal power for 20 s, 1 min pause, on ice). The suspension was centrifuged for 1 h at 22,000 g and 4 °C. The pellet, containing Opa60 inclusion bodies, was resuspended in 30 ml lysis buffer with 1% w/v Triton X-100, and again centrifuged for 1 h at 22,000 g and 4 °C. This step was repeated without Triton X-100, and the pellet was resuspended in 50 ml solubilization buffer (50 mM Tris, 150 mM NaCl, 6 M guanidinium hydrochloride (Gmd-HCl), pH 8.0). Non-solubilized particles were removed by centrifugation for 45 min at 25,000 g and 22 °C. 2 mM imidazole was added to the supernatant, and this was loaded at room temperature onto a 5 ml column volume (CV) TALON resin (Takara Bio) affinity column, equilibrated in loading buffer (20 mM sodium phosphate, 150 mM NaCl, 6 M Gmd-HCl, 2 mM imidazole, pH 7.8). The resin was washed with 3 CV wash buffer (loading buffer supplemented with 10 mM imidazole), and finally, Opa60 was eluted with 4 CV of elution buffer (loading buffer supplemented with 250 mM imidazole). A sodium dodecyl sulfate–polyacrylamide gel electrophoresis (SDS-PAGE) analysis of the affinity purification is shown in Figure S1. Solubilized Opa60 was refolded for 2.5 days at room temperature by 40-fold dilution from ~2.5–5 mg/ml protein concentration into refolding buffer (20 mM Tris, 500 mM NaCl, 0.25 % w/v DPC, pH 8.0, cOmplete™ EDTA-free protease inhibitor cocktail (Roche)). Folding success was assessed with SDS-PAGE shift (de Jonge et al., 2002). Refolded protein was concentrated and further purified by size exclusion chromatography (SEC, Superdex™ 200 Increase 10/300 GL (GE Healthcare), SEC buffer (20 mM sodium phosphate, 150 mM NaCl, 0.15% w/v DPC, pH 6.2), room temperature, flow rate 0.75 ml/min, each run loading ~ 0.8 ml of protein solution). Opa60-containing fractions were pooled.

Opa60 was reconstituted into 1,2-dimyristoyl-*sn*-glycero-3-phosphocholine (DMPC, Avanti Polar Lipids) lipid bilayers by dialysis against dialysis buffer (20 mM sodium phosphate, 100 mM NaCl, 20 mM $MgCl_2$, pH 6.2). DPC-solubilized protein was added together with DMPC at a lipid-to-protein (LPR) mass ratio of 0.25 or 0.33 (10 to 13.5 molar LPR) into a dialysis cassette (cutoff 3,500 Da, volume 1–5 ml), and the buffer (500 ml volume) was changed each day for 5 days. Methyl-β-cyclodextrin was added at 5–10 mg per mg Opa60 to the dialysis buffer to accelerate the process on days 1–3, but was not in the final 2 dialysis buffer changes. After successful reconstitution (white precipitate), 0.02% w/v NaN_3 was added to the final sample. Opa60 in DMPC bilayers was packed into a 1.3 mm MAS NMR rotor (Bruker) via centrifugation (Bockmann et al., 2009). Note that a spectrum with LPR of 0.5 was also initially recorded (Figure S2) and overlays well with the spectrum at LPR of 0.25, with small changes in chemical shift. We therefore proceeded with the samples at 0.25 or 0.33 LPR for assignments and structure determination.

Uniformly ^{13}C, ^{15}N labelled Opa60 was prepared according to the same protocol, but was reconstituted into deuterated DMPC (DMPC-d_{54}, Avanti Polar Lipids) with an LPR of 0.25. The sample was packed into a 0.7 mm MAS NMR rotor (Bruker).

For samples of Opa60 in different lipids, perdeuterated protein was reconstituted in Kdo2-Lipid A (KLA, Sigma-Aldrich) (Kucharska et al., 2016), Rd2 lipopolysaccharide (LPS, Sigma-Aldrich) from *E. coli* F583 (Kucharska et al., 2016) and LPS from *E. coli* K235 (Sigma-Aldrich). The LPR was adjusted such that the number of acyl chains remained the same when compared to DMPC.

hCEACAM1-N** sample **preparation

The procedure for expression and purification of human CEACAM1 (hCEACAM1-N) is based on a previously published procedure (Fedarovich et al., 2006). A pGEX-4 T-1 plasmid containing the sequence for expression of the N-terminal domain (12 kDa) of hCEACAM1-N was transformed into *Escherichia coli* BL21 (DE3) cells. The construct contained an N-terminal GST-tag fused to hCEACAM1-N via a thrombin cleavage site. ^{15}N labelled hCEACAM1-N was expressed in M9 medium (1 g/l ^{15}N-NH_4Cl). Cells were grown at 37 °C until the OD_{600} reached 0.6–0.7. The temperature was then decreased to 25 °C before induction of expression with 0.5 mM IPTG. Expression was conducted overnight, and cells were harvested by centrifugation for 20 min at 5,000 g and 4 °C.

The pellet was resuspended in 35 ml lysis buffer (40 mM Tris, 150 mM NaCl, 2 mM EDTA, 10% v/v glycerol, 2 mM DTT, 1 mM PMSF, pH 8.0). Cells were lysed by sonication (Sonopuls HD 2200 (Bandelin), 3x20% of maximum power for 20 s, 1-minute pause, on ice) and passage through Emulsiflex–C3 (Avestin) at 1,000 psi. Lysate was centrifuged for 15 min at 7,000 g and 4 °C and subsequently the supernatant was centrifuged for 30 min at 22,000 g and 4 °C. The supernatant of the second centrifugation step was loaded onto a 5 ml GS-Trap™ HP column (Sigma-Aldrich). After washing the column, GST-hCEACAM1-N was eluted with elution buffer (40 mM Tris, 150 mM NaCl, 2 mM EDTA, 10% v/v glycerol, 2 mM DTT, 20 mM reduced glutathione, pH 8.0) at 1 ml/min. Fractions of 2 ml were collected and assessed for GST-hCEACAM1-N with SDS–PAGE. Positive fractions were pooled and thrombin (Sigma–Aldrich) was added at 10 U per mg GST-hCEACAM1-N. Cleavage was conducted for 2.5 days at room temperature. The mixture was then concentrated and hCEACAM1-N was purified via gel filtration on a Superdex™ 75 10/300 GL column (GE Healthcare) with SEC buffer (20 mM sodium phosphate, 150 mM NaCl, pH 6.2) at a flow rate of 0.7 ml/min. 1 ml fractions were collected and assessed for hCEACAM1-N content. Fractions containing the protein were pooled and concentrated for

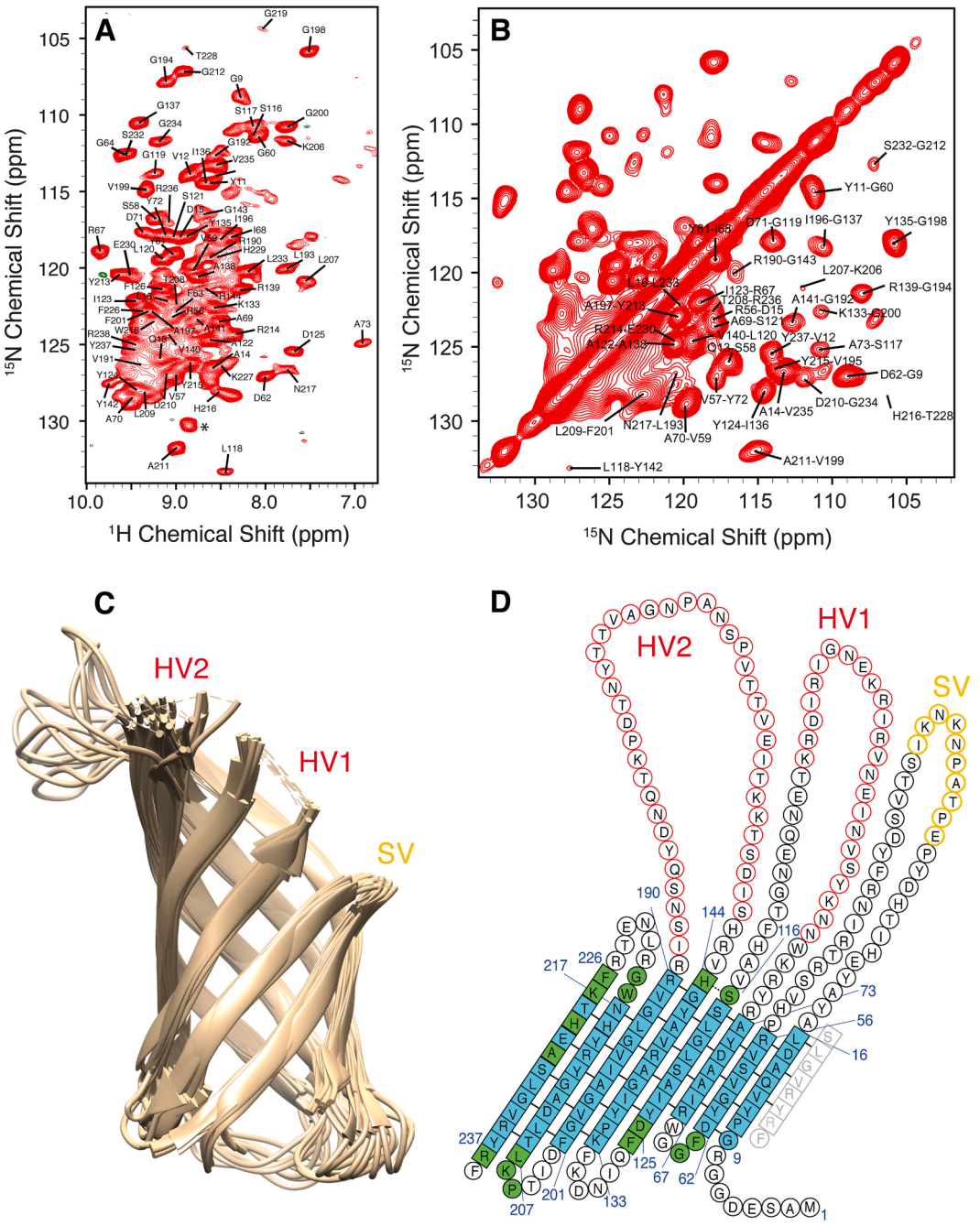

Fig. 1. The structure of Opa60 in lipid bilayers. (A) Cross-polarization-based ^{1}H-^{15}N correlation spectrum with assignments annotated for the majority of the resonances. * indicates an aliased peak from arginine side chain. (B) Projection of the 4D HN(H)(H)NH spectrum and the assigned proton-proton contacts, which are primarily from one beta strand to another. (C) Structure of the beta barrel of Opa60. The 10 lowest energy structures from the CYANA structure calculation are shown. Loop regions are not shown. The location of the loops (SV, HV1, and HV2) are indicated in yellow and red. Where there is a gap in the displayed residues, dashed lines connect residues of the same model. (D) Topology map of Opa60. Residues in a beta strand conformation are indicated by squares, loop residues by circles. Green and blue residues are assigned (at least amide N and HN, except proline), and for blue residues, contacts in the 4D HN(H)(H)NH spectrum were found and included as hydrogen bond restraints in the structure calculation. HV and SV regions are indicated in red and yellow, respectively. (For interpretation of the references to colour in this figure legend, the reader is referred to the web version of this article.)

NMR spectroscopy. SDS-PAGE analysis of hCEACAM1-N production is shown in figures S3-S5.

NMR spectroscopy

Assignment spectra (Barbet-Massin et al., 2013; Barbet-Massin et al., 2014) of perdeuterated Opa60 were recorded on 600 MHz (Bruker 600 UltraShield, 14.1 T field strength with a Bruker MASDVT600W2 BL1.3 HXY probe) and 800 MHz (Bruker 800US2, 18.8 T field strength with a Bruker MASDVT800S6 BL1.3 HCN probe) spectrometers. The MAS rate was 55 kHz and the temperature was set to 240 K, resulting in a sample temperature of about 298 K determined using the chemical shift of water (Bockmann et al., 2009). Alpha proton assignments (Stanek et al., 2016) were extended from these assignments at a Bruker 950 MHz spectrometer using a 0.7 mm probe (Bruker 950US2, 22.3 T field strength with a Bruker MASDVT950S6 BL0.7 N/D/C/H probe) using uniformly ^{13}C, ^{15}N

labelled Opa60. Recording conditions for all spectra are given in Tables S1-2.

In all spectra, heteronuclear decoupling was applied on the proton channel as swept frequency TPPM (Thakur et al., 2006; Bennett et al., 1995) at about 12 kHz and on carbon or nitrogen channels as WALTZ-16 (Shaka et al., 1983) with 10 kHz. The water suppression scheme was MISSISSIPPI (Zhou and Rienstra, 2008) applied for 100–200 ms with a strength corresponding to a quarter of the MAS rate.

Structure calculation

The structure was determined using CYANA (Guntert and Buchner, 2015; Guntert et al., 1997) 68 hydrogen bond restraints (Pauling and Corey, 1951) were derived from the 34 proton-proton contacts in the HN(H)(H)NH spectrum and manually entered as upper and lower distance restraints as given in Table S4. A single weak contact from S116 to H144 was entered as an HN-HN upper distance limit of 4 Å. Backbone torsion angles were predicted with TALOS-N (Shen and Bax, 2013) and entered into the structure calculation with a range of 40 degrees or ± 2 times the estimated error from TALOS-N, whichever was larger. 2000 structures were calculated with CYANA and the 10 lowest energy structures were included in the final ensemble. CYANA target function ranged from 0.18 to 0.62. The calculation of a large number of structures was necessary to avoid violations, which otherwise occurred in both the restrained and the unrestrained part of the protein. The resulting structural ensemble was analyzed with UCSF Chimera 1.14 (Pettersen et al., 2004) and the backbone RMSD in the well–defined beta barrel (residues 9–16, 56–62, 67–73, 113–125, 133–144, 190–201, 207–217, 225–237) was 0.6 Å. The coordinates were deposited at the Protein Data Bank under the code 8QWQ.

Data analysis and resonance assignment

Spectra were processed using Bruker TopSpin 3.5.7 and 4.0.8. Data was corrected for linear field drift (Najbauer and Andreas, 2019). Apodization was applied using the QSINE function with a sine bell shift of 2 (cosine squared apodization). All chemical shifts were referenced using the methyl resonance of sodium 2,2-dimethyl-2-silapentane-5-sulfonate (DSS) set to zero (in an external reference), and using frequency ratios for referencing of ^{13}C and ^{15}N on the DSS and liquid ammonia scales, respectively (Harris et al., 2008). The assignment was performed using NMRFAM-SPARKY (Lee et al., 2015). After an initial automated assignment using FLYA (Schmidt and Guntert, 2012), the assignment was manually confirmed and extended.

The resulting assignments from the perdeuterated sample for backbone atoms HN, N, CA, CB, and CO are reported in BMRB entry 34872. Proton alpha resonances, determined from the protonated sample, are reported in Table S3. H^{α}-H^{α} contacts found were between D15 – G234, Y72 – L118, P134 – V199, I136 – A197 and V140 – L193.

Results and discussion

We prepared [^{2}H,^{13}C,^{15}N]-Opa60 in DMPC bilayers and obtained sufficient spectral quality for resonance assignment and structure determination (Fig. 1). For resonance assignment, we recorded a set of proton-detected 3-dimensional spectra connecting CA, CB, and CO frequencies (Barbet-Massin et al., 2013; Barbet-Massin et al., 2014). An additional spectrum was used to confirm ^{H}N–^{H}N connectivity (Table S1) (Andreas et al., 2015). All these spectra are based on linking the amide resonances in the ^{15}N–^{1}H correlation spectrum (Fig. 1A), with resonances of neighboring residues. Once assigned, the amide resonances are key to determination of the beta strand arrangement via correlations in the 4D HN(H)(H)NH spectrum, a projection of which is shown in Fig. 1B. The MAS NMR structure of Opa60 is shown in Fig. 1C. We used peak lists from the experiments listed in Table S1 as an input to the FLYA module of the CYANA software package, which uses a genetic algorithm to obtain automated assignments (Schmidt and Guntert, 2012). These were then manually confirmed and extended to a total of 84 residues within the beta barrel region of Opa60 (Fig. 1D, Table S3). A strip plot demonstrating the assignment process for CA linking is shown in Figure S6. In comparison to assignments obtained in DPC detergent micelles (Fox et al., 2014), we were able to extend assignments by 3 residues in beta strands 4 and 5, and 6 residues in strands 7 and 8 in the direction of the large disordered loops. This likely highlights the denaturing effects of detergent for residues outside the membrane (Schubeis et al., 2020), but may also reflect differing local dynamics for these residues, considering also that solution NMR and MAS NMR are not equally influenced by relaxation. Residues in the shorter loops on the other side of the barrel remain unassigned in DMPC bilayers although they could be assigned in detergent micelles. This can be explained by differing sensitivity of the measurements towards structural dynamics: dynamic residues can often be more easily detected in solution NMR, yet are absent from CP-based MAS NMR spectra (Matlahov and van der Wel, 2018; Andreas et al., 2010; Andreas et al., 2015; Schnell and Chou, 2008). We were unable to assign residues belonging to the large extracellular loops in either CP- or INEPT-based spectra, which again can be explained by a high degree of flexibility on the nanosecond-millisecond timescale. In a previous study, only some loop residues could be assigned in detergent micelles, in particular a stretch of 17 residues in the HV2 loop, which were assigned with the help of a synthetic peptide (Fox et al., 2014).

The MAS NMR structure of Opa60 was determined primarily from hydrogen bonds inferred from proton proximities detected in the HN(H)(H)NH spectrum (Fig. 1B), defining the beta barrel topology (Fig. 1D). The 34 assigned amide correlations were used to define 68 beta sheet hydrogen bond restraints (Pauling and Corey, 1951), and were entered manually into the structure calculation. An additional weak correlation between residues H144 and S116 was observed, and thus a 4 Å upper distance limit was introduced between the amide protons of these residues. We also included TALOS-N (Shen and Bax, 2013) angle restraints (Tables S5 and 6) into the CYANA structure calculation (Guntert and Buchner, 2015; Guntert et al., 1997). Additionally, we obtained assignments of H^{α} protons from a fully protonated sample of Opa60 (Tables S2 and S4) and found 5 H^{α}-H^{α} contacts in the 3 dimensional (H)C(H)(H)CH spectrum, (recorded as co-acquired with an (H)N(H)(H)NH spectrum) (Linser et al., 2014). One selected example of an HN-HN and an H^{α}-H^{α} contact is shown in Figure S7, along with the molecular structure showing the proton-proton distances that occur in the antiparallel beta sheet arrangement.

The structure of the beta barrel of Opa60 is shown in Fig. 1C after truncation of the large SV and HV loops, which could not be assigned. The backbone RMSD of the 10 lowest energy structures aligned in the beta barrel region (residues 9–16, 56–62, 67–73, 113–125, 133–144, 190–201, 207–217, 225–237) is below 1 Å. The strand arrangement in the transmembrane structure agrees with the detergent micelle structure reported previously (Fox et al., 2014), with only minor additional structuring observed towards the end of beta strands connecting to the extracellular loops. This is in contrast to our work on the protein AlkL, in which the structure of loop residues was disrupted by detergent, but formed in DMPC lipids (Schubeis et al., 2020). Similar to Opa60, lipid bilayer preparations of outer membrane protein A from *Klebsiella pneumoniae* (KpOmpA) resulted in MAS spectra with strong signals arising from the relatively rigid beta barrel domain, but loop residues that were not assigned due to intermediate timescale motions (Saurel et al., 2017). The loops of KpOmpA have been proposed to play a role in cell adhesion.

The lipid bilayer preparations are a starting point to investigate interactions with CEACAM proteins. Our initial attempts to reproduce the nanomolar binding of the N-terminal domain of hCEACAM1 (described recently for recombinant protein in a lipid mixture that included polyethylene glycol functionalized lipid (Martin et al., 2016)) were not successful, suggesting that a careful optimization of conditions, or expression to cellular membranes or extramembrane vesicles (Meuskens

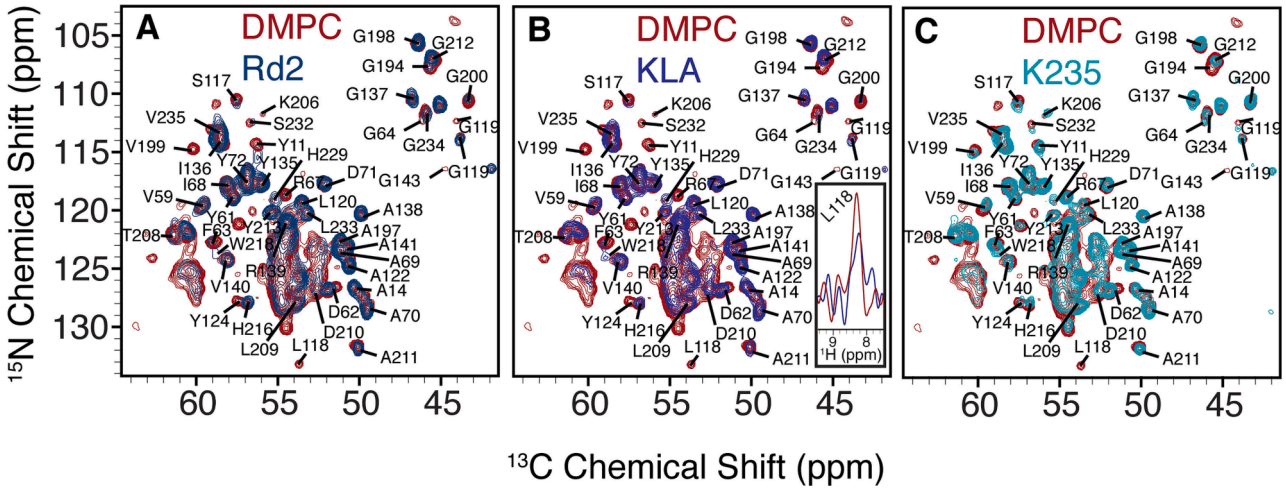

Fig. 2. CA-N projections from 3D (H)CANH spectra of Opa60 in different lipid environments, DMPC (dark red), *E. Coli* Rd2 LPS (A, dark blue), KLA (B, blue) and *E. Coli* K235 LPS (C, turquois). The inset in (B) shows the signal-to-noise ratio for a slice taken at L118, which is one of the weaker peaks. Spectra were recorded at an 800 MHz spectrometer, with 55 kHz MAS. (For interpretation of the references to colour in this figure legend, the reader is referred to the web version of this article.)

et al., 2017; Shahid et al., 2015; Thoma et al., 2018), may be necessary. Future studies are expected to elucidate the binding interaction between Opa60 and the CEACAM proteins. This will then be assessed in the context of other proteins of pathogenic bacteria which have evolved to exploit the CEACAM proteins as an entry into human hosts (Bonsor et al., 2018; Conners et al., 2008; Korotkova et al., 2008; Tchoupa et al., 2015). The spectrum of the N-terminal domain of human CEACAM1 is shown in Figure S8.

The lipid bilayer environment has been shown to have an impact on membrane protein structure and function (Chipot et al., 2018; Schubeis et al., 2020; Zhou and Cross, 2013). Since Opa60 exhibits flexible loops even in DMPC membranes, we wondered whether the native outer membrane lipids of *N. gonorrhoeae* might stabilize the loops. While the lipooligosaccharides (LOS) forming most of the outer membrane are not commercially available, Kdo2-Lipid A (KLA) is an excellent substitute, as it closely resembles the core region of the LOS. We also prepared samples in two varieties of lipopolysaccharides (LPS) found in the *Escherichia coli* strains K235 and F583 (Rd2). Interactions between the extracellular loops of OprH and LPS were detected before in a detergent environment based on solution NMR chemical shift perturbations (Kucharska et al., 2016). Reconstituted samples of LPS do not assemble as the asymmetric native lipid bilayer, but might allow important interactions to form between the loops and LOS moieties. However, we find no striking difference in either the chemical shifts (Fig. 2) or the peak intensities in the four lipid bilayers, indicating that Opa60's conformation and mobility are largely unchanged, and revealing that the loops remain mobile upon the addition of such lipids. Note that minor differences in peak intensity observed in the spectrum of Fig. 2 result in the apparent loss of several resonances in the projection. These peaks are typically still found in the 3D spectrum, as shown for the case of L118 in the inset to panel B: the change in intensity between the DMPC spectrum and the KLA spectrum is within the range expected given the noise level, but this results in the KLA peak falling below the threshold used for contouring of the N-C projection.

Conclusions

In conclusion, we determined the membrane-bound structure of Opa60 using only data from lipid bilayers. We determined that Opa60 has the same strand alignment in lipid bilayers as it does in detergent micelles, and we found additional structuring in several loop residues that extends the transmembrane structure. Consistent with the detergent conditions, the large loops known to interact with host factors were found to be unstructured. This reported structure of Opa60 joins a handful of beta barrel protein structures determined to date by MAS NMR.

CRediT authorship contribution statement

Marcel C. Forster: Investigation, Writing – original draft. **Kumar Tekwani Movellan:** Visualization, Writing – review & editing. **Eszter E. Najbauer:** Visualization, Writing – review & editing. **Stefan Becker:** Resources, Validation, Writing – review & editing. **Loren B. Andreas:** Conceptualization, Funding acquisition, Resources, Supervision, Writing – review & editing.

Declaration of competing interest

The authors declare that they have no known competing financial interests or personal relationships that could have appeared to influence the work reported in this paper.

Data availability

Chemical shifts have been deposited at the Biological Magnetic Resonance Bank (entry 34872). The solid-state NMR structure coordinates are deposited at the Protein Data Bank under the code 8QWQ.

Acknowledgments

The authors acknowledge financial support from the MPI for Multidisciplinary Sciences, and from the Deutsche Forschungsgemeinschaft (Emmy Noether program Grant AN1316). They thank Claudia Schwiegk for excellent help with the synthesis and purification of hCEACAM1-N. They also thank Dr. Dirk Bockelmann and Brigitta Angerstein for technical assistance.

Appendix A. Supplementary data

Supplementary data to this article can be found online at https://doi.org/10.1016/j.yjsbx.2024.100098.

References

Andreas, L.B., Eddy, M.T., Pielak, R.M., Chou, J., Griffin, R.G., 2010. Magic angle spinning NMR investigation of influenza A M2(18–60): support for an allosteric mechanism of inhibition. J. Am. Chem. Soc. 132 (32), 10958–10960.

Andreas, L.B., Reese, M., Eddy, M.T., Gelev, V., Ni, Q.Z., Miller, E.A., Emsley, L., Pintacuda, G., Chou, J.J., Griffin, R.G., 2015. Structure and mechanism of the influenza A M218–60 dimer of dimers. J. Am. Chem. Soc. 137 (47), 14877–14886.
Andreas, L.B., Stanek, J., Le Marchand, T., Bertarello, A., Cala-De Paepe, D., Lalli, D., Krejcikova, M., Doyen, C., Oster, C., Knott, B., Wegner, S., Engelke, F., Felli, I.C., Pierattelli, R., Dixon, N.E., Emsley, L., Herrmann, T., Pintacuda, G., 2015. Protein residue linking in a single spectrum for magic-angle spinning NMR assignment. J. Biomol. NMR 62 (3), 253–261.
Barbet-Massin, E., Pell, A.J., Jaudzems, K., Franks, W.T., Retel, J.S., Kotelovica, S., Akopjana, I., Tars, K., Emsley, L., Oschkinat, H., Lesage, A., Pintacuda, G., 2013. Out-and-back 13C–13C scalar transfers in protein resonance assignment by proton-detected solid-state NMR under ultra-fast MAS. J. Biomol. NMR 56 (4), 379–386.
Barbet-Massin, E., Pell, A.J., Retel, J.S., Andreas, L.B., Jaudzems, K., Franks, W.T., Nieuwkoop, A.J., Hiller, M., Higman, V., Guerry, P., Bertarello, A., Knight, M.J., Felletti, M., Le Marchand, T., Kotelovica, S., Akopjana, I., Tars, K., Stoppini, M., Bellotti, V., Bolognesi, M., Ricagno, S., Chou, J.J., Griffin, R.G., Oschkinat, H., Lesage, A., Emsley, L., Herrmann, T., Pintacuda, G., 2014. Rapid proton-detected NMR assignment for proteins with fast magic angle spinning. J. Am. Chem. Soc. 136 (35), 12489–12497.
Bennett, A.E., Rienstra, C.M., Auger, M., Lakshmi, K.V., Griffin, R.G., 1995. Heteronuclear decoupling in rotating solids. J. Chem. Phys. 103 (16), 6951–6958.
Bockmann, A., Gardiennet, C., Verel, R., Hunkeler, A., Loquet, A., Pintacuda, G., Emsley, L., Meier, B.H., Lesage, A., 2009. Characterization of different water pools in solid-state NMR protein samples. J. Biomol. NMR 45 (3), 319–327.
Bonsor, D.A., Zhao, Q., Schmidinger, B., Weiss, E., Wang, J., Deredge, D., Beadenkopf, R., Dow, B., Fischer, W., Beckett, D., Wintrode, P.L., Haas, R., Sundberg, E.J., 2018. The Helicobacter pylori adhesin protein HopQ exploits the dimer interface of human CEACAMs to facilitate translocation of the oncoprotein CagA. EMBO J. 37 (13).
Bos, M.P., Kao, D., Hogan, D.M., Grant, C.C., Belland, R.J., 2002. Carcinoembryonic antigen family receptor recognition by gonococcal Opa proteins requires distinct combinations of hypervariable Opa protein domains. Infect. Immun. 70 (4), 1715–1723.
Cheng, Y., 2018. Membrane protein structural biology in the era of single particle cryo-EM. Curr. Opin. Struct. Biol. 52, 58–63.
Chipot, C., Dehez, F., Schnell, J.R., Zitzmann, N., Pebay-Peyroula, E., Catoire, L.J., Miroux, B., Kunji, E.R.S., Veglia, G., Cross, T.A., Schanda, P., 2018. Perturbations of native membrane protein structure in alkyl phosphocholine detergents: a critical assessment of NMR and biophysical studies. Chem. Rev. 118 (7), 3559–3607.
Conners, R., Hill, D.J., Borodina, E., Agnew, C., Daniell, S.J., Burton, N.M., Sessions, R.B., Clarke, A.R., Catto, L.E., Lammie, D., Wess, T., Brady, R.L., Virji, M., 2008. The Moraxella adhesin UspA1 binds to its human CEACAM1 receptor by a deformable trimeric coiled-coil. EMBO J. 27 (12), 1779–1789.
Cournia, Z., Allen, T.W., Andricioaei, I., Antonny, B., Baum, D., Brannigan, G., Buchete, N.V., Deckman, J.T., Delemotte, L., Del Val, C., Friedman, R., Gkeka, P., Hege, H.C., Henin, J., Kasimova, M.A., Kolocouris, A., Klein, M.L., Khalid, S., Lemieux, M.J., Lindow, N., Roy, M., Selent, J., Tarek, M., Tofoleanu, F., Vanni, S., Urban, S., Wales, D.J., Smith, J.C., Bondar, A.N., 2015. Membrane protein structure, function, and dynamics: a perspective from experiments and theory. J. Membr. Biol. 248 (4), 611–640.
Criss, A.K., Seifert, H.S., 2012. A bacterial siren song: intimate interactions between Neisseria and neutrophils. Nat. Rev. Microbiol. 10 (3), 178–190.
de Jonge, M.I., Bos, M.P., Hamstra, H.J., Jiskoot, W., van Ulsen, P., Tommassen, J., van Alphen, L., van der Ley, P., 2002. Conformational analysis of opacity proteins from Neisseria meningitidis. Eur. J. Biochem. 269 (21), 5215–5223.
de Jonge, M.I., Hamstra, H.J., van Alphen, L., Dankert, J., van der Ley, P., 2003. Mapping the binding domains on meningococcal Opa proteins for CEACAM1 and CEA receptors. Mol. Microbiol. 50 (3), 1005–1015.
Fedarovich, A., Tomberg, J., Nicholas, R.A., Davies, C., 2006. Structure of the N-terminal domain of human CEACAM1: binding target of the opacity proteins during invasion of Neisseria meningitidis and N. gonorrhoeae. Acta Crystallogr. D Biol. Crystallogr. 62 (Pt 9), 971–979.
Fox, D.A., Columbus, L., 2013. Solution NMR resonance assignment strategies for beta-barrel membrane proteins. Protein Sci. 22 (8), 1133–1140.
Fox, D.A., Larsson, P., Lo, R.H., Kroncke, B.M., Kasson, P.M., Columbus, L., 2014. Structure of the Neisserial outer membrane protein Opa(6)(0): loop flexibility essential to receptor recognition and bacterial engulfment. J. Am. Chem. Soc. 136 (28), 9938–9946.
Galdiero, S., Galdiero, M., Pedone, C., 2007. beta-Barrel membrane bacterial proteins: structure, function, assembly and interaction with lipids. Curr. Protein Pept. Sci. 8 (1), 63–82.
Gray-Owen, S.D., 2003. Neisserial Opa proteins: impact on colonization, dissemination and immunity. Scand. J. Infect. Dis. 35 (9), 614–618.
Guntert, P., Buchner, L., 2015. Combined automated NOE assignment and structure calculation with CYANA. J. Biomol. NMR 62 (4), 453–471.
Guntert, P., Mumenthaler, C., Wuthrich, K., 1997. Torsion angle dynamics for NMR structure calculation with the new program DYANA. J. Mol. Biol. 273 (1), 283–298.
Harris, R.K., Becker, E.D., Menezes, S.M.C., 2008. Further conventions for NMR shielding and chemical shifts (IUPAC recommendations 2008). Pure Appl. Chem. 80 (1), 59–84.
Hauck, C.R., Meyer, T.F., 2003. 'Small' talk: Opa proteins as mediators of Neisseria-host-cell communication. Curr. Opin. Microbiol. 6 (1), 43–49.
Hobbs, M.M., Seiler, A., Achtman, M., Cannon, J.G., 1994. Microevolution within a clonal population of pathogenic bacteria: recombination, gene duplication and horizontal genetic exchange in the opa gene family of Neisseria meningitidis. Mol. Microbiol. 12 (2), 171–180.
Korotkova, N., Yang, Y., Le Trong, I., Cota, E., Demeler, B., Marchant, J., Thomas, W.E., Stenkamp, R.E., Moseley, S.L., Matthews, S., 2008. Binding of Dr adhesins of Escherichia coli to carcinoembryonic antigen triggers receptor dissociation. Mol. Microbiol. 67 (2), 420–434.
Kucharska, I., Liang, B., Ursini, N., Tamm, L.K., 2016. Molecular interactions of lipopolysaccharide with an outer membrane protein from pseudomonas aeruginosa probed by solution NMR. Biochemistry 55 (36), 5061–5072.
Kwan, T.O.C., Axford, D., Moraes, I., 2020. Membrane protein crystallography in the era of modern structural biology. Biochem. Soc. Trans. 48 (6), 2505–2524.
Lee, W., Tonelli, M., Markley, J.L., 2015. NMRFAM-SPARKY: enhanced software for biomolecular NMR spectroscopy. Bioinformatics 31 (8), 1325–1327.
Linser, R., Bardiaux, B., Andreas, L.B., Hyberts, S.G., Morris, V.K., Pintacuda, G., Sunde, M., Kwan, A.H., Wagner, G., 2014. Solid-state NMR structure determination from diagonal-compensated, sparsely nonuniform-sampled 4D proton-proton restraints. J. Am. Chem. Soc. 136 (31), 11002–11010.
Malorny, B., Morelli, G., Kusecek, B., Kolberg, J., Achtman, M., 1998. Sequence diversity, predicted two-dimensional protein structure, and epitope mapping of neisserial Opa proteins. J. Bacteriol. 180 (5), 1323–1330.
Mandala, V.S., Williams, J.K., Hong, M., 2018. Structure and dynamics of membrane proteins from solid-state NMR. Annu. Rev. Biophys. 47, 201–222.
Martin, J.N., Ball, L.M., Solomon, T.L., Dewald, A.H., Criss, A.K., Columbus, L., 2016. Neisserial opa protein-CEACAM interactions: competition for receptors as a means of bacterial invasion and pathogenesis. Biochemistry 55 (31), 4286–4294.
Matlahov, I., van der Wel, P.C.A., 2018. Hidden motions and motion-induced invisibility: dynamics-based spectral editing in solid-state NMR. Methods 148, 123–135.
Meuskens, I., Michalik, M., Chauhan, N., Linke, D., Leo, J.C., 2017. A new strain collection for improved expression of outer membrane proteins. Front. Cell. Infect. Microbiol. 7, 464.
Najbauer, E.E., Andreas, L.B., 2019. Correcting for magnetic field drift in magic-angle spinning NMR datasets. J. Magn. Reson. 305, 1–4.
Overington, J.P., Al-Lazikani, B., Hopkins, A.L., 2006. How many drug targets are there? Nat. Rev. Drug Discov. 5 (12), 993–996.
Pauling, L., Corey, R.B., 1951. Configurations of polypeptide chains with favored orientations around single bonds: two new pleated sheets. PNAS 37 (11), 729–740.
Pettersen, E.F., Goddard, T.D., Huang, C.C., Couch, G.S., Greenblatt, D.M., Meng, E.C., Ferrin, T.E., 2004. UCSF Chimera–a visualization system for exploratory research and analysis. J. Comput. Chem. 25 (13), 1605–1612.
Raetz, C.R., Whitfield, C., 2002. Lipopolysaccharide endotoxins. Annu. Rev. Biochem 71, 635–700.
Saurel, O., Iordanov, I., Nars, G., Demange, P., Le Marchand, T., Andreas, L.B., Pintacuda, G., Milon, A., 2017. Local and global dynamics in klebsiella pneumoniae outer membrane protein a in lipid bilayers probed at atomic resolution. J. Am. Chem. Soc. 139 (4), 1590–1597.
Schanda, P., Ernst, M., 2016. Studying dynamics by magic-angle spinning solid-state NMR spectroscopy: principles and applications to biomolecules. Prog Nucl Mag Res Sp 96, 1–46.
Schmidt, E., Guntert, P., 2012. A new algorithm for reliable and general NMR resonance assignment. J. Am. Chem. Soc. 134 (30), 12817–12829.
Schnell, J.R., Chou, J.J., 2008. Structure and mechanism of the M2 proton channel of influenza A virus. Nature 451 (7178), 591–595.
Schubeis, T., Le Marchand, T., Andreas, L.B., Pintacuda, G., 2018. (1)H magic-angle spinning NMR evolves as a powerful new tool for membrane proteins. J. Magn. Reson. 287, 140–152.
Schubeis, T., Le Marchand, T., Daday, C., Kopec, W., Tekwani Movellan, K., Stanek, J., Schwarzer, T.S., Castiglione, K., de Groot, B.L., Pintacuda, G., Andreas, L.B., 2020. A beta-barrel for oil transport through lipid membranes: dynamic NMR structures of AlkL. PNAS 117 (35), 21014–21021.
Shahid, S.A., Nagaraj, M., Chauhan, N., Franks, T.W., Bardiaux, B., Habeck, M., Orwick-Rydmark, M., Linke, D., van Rossum, B.J., 2015. Solid-state NMR study of the YadA membrane-anchor domain in the bacterial outer membrane. Angew. Chem. Int. Ed. Engl. 54 (43), 12602–12606.
Shaka, A.J., Keeler, J., Frenkiel, T., Freeman, R. An improved sequence for broadband decoupling: WALTZ-16. Journal of Magnetic Resonance (1969) **1983,** 52 (2), 335-338.
Shen, Y., Bax, A., 2013. Protein backbone and sidechain torsion angles predicted from NMR chemical shifts using artificial neural networks. J. Biomol. NMR 56 (3), 227–241.
Sohlenkamp, C., Geiger, O., 2016. Bacterial membrane lipids: diversity in structures and pathways. FEMS Microbiol. Rev. 40 (1), 133–159.
Stanek, J., Andreas, L.B., Jaudzems, K., Cala, D., Lalli, D., Bertarello, A., Schubeis, T., Akopjana, I., Kotelovica, S., Tars, K., Pica, A., Leone, S., Picone, D., Xu, Z.Q., Dixon, N.E., Martinez, D., Berbon, M., El Mammeri, N., Noubhani, A., Saupe, S., Habenstein, B., Loquet, A., Pintacuda, G., 2016. NMR spectroscopic assignment of backbone and side-chain protons in fully protonated proteins: microcrystals, sedimented assemblies, and amyloid fibrils. Angew. Chem. Int. Ed. Engl. 55 (50), 15504–15509.
Tamm, L.K., Liang, B.Y., 2006. NMR of membrane proteins in solution. Prog Nucl Mag Res Sp 48 (4), 201–210.
Tchoupa, A.K., Lichtenegger, S., Reidl, J., Hauck, C.R., 2015. Outer membrane protein P1 is the CEACAM-binding adhesin of Haemophilus influenzae. Mol. Microbiol. 98 (3), 440–455.
Thakur, R.S., Kurur, N.D., Madhu, P.K., 2006. Swept-frequency two-pulse phase modulation for heteronuclear dipolar decoupling in solid-state NMR. Chem. Phys. Lett. 426 (4), 459–463.
Thakur, N., Ray, A.P., Sharp, L., Jin, B., Duong, A., Pour, N.G., Obeng, S., Wijesekara, A. V., Gao, Z.G., McCurdy, C.R., Jacobson, K.A., Lyman, E., Eddy, M.T., 2023. Anionic

phospholipids control mechanisms of GPCR-G protein recognition. Nat. Commun. 14 (1), 794.
Thoma, J., Manioglu, S., Kalbermatter, D., Bosshart, P.D., Fotiadis, D., Muller, D.J., 2018. Protein-enriched outer membrane vesicles as a native platform for outer membrane protein studies. Commun. Biol. 1, 23.
Werner, L.M., Palmer, A., Smirnov, A., Belcher Dufrisne, M., Columbus, L., Criss, A.K., 2020. Imaging flow cytometry analysis of CEACAM binding to opa-expressing neisseria gonorrhoeae. Cytometry A 97 (10), 1081–1089.
Wilkinson, S.G., 1996. Bacterial lipopolysaccharides–themes and variations. Prog. Lipid Res. 35 (3), 283–343.
Wimley, W.C., 2003. The versatile beta-barrel membrane protein. Curr. Opin. Struct. Biol. 13 (4), 404–411.
Xue, K., Movellan, K.T., Zhang, X.C., Najbauer, E.E., Forster, M.C., Becker, S., Andreas, L. B., 2021. Towards a native environment: structure and function of membrane proteins in lipid bilayers by NMR. Chem. Sci. 12 (43), 14332–14342.
Zhang, X.C., Forster, M.C., Nimerovsky, E., Movellan, K.T., Andreas, L.B., 2021. Transferred-rotational-echo double resonance. Chem. A Eur. J. 125 (3), 754–769.
Zhou, H.X., Cross, T.A., 2013. Influences of membrane mimetic environments on membrane protein structures. Annu. Rev. Biophys. 42, 361–392.
Zhou, D.H., Rienstra, C.M., 2008. High-performance solvent suppression for proton detected solid-state NMR. J. Magn. Reson. 192 (1), 167–172.